

# Cluster and then Embed: A Modular Approach for Visualization

Elizabeth Coda<sup>1</sup>, Ery Arias-Castro<sup>1,2</sup>, and Gal Mishne<sup>2</sup>

<sup>1</sup>Department of Mathematics, University of California, San Diego

<sup>2</sup>Halıcıoğlu Data Science Institute, University of California, San Diego

## Abstract

Dimensionality reduction methods such as t-SNE and UMAP are popular methods for visualizing data with a potential (latent) clustered structure. They are known to group data points at the same time as they embed them, resulting in visualizations with well-separated clusters that preserve local information well. However, t-SNE and UMAP also tend to distort the global geometry of the underlying data. We propose a more transparent, modular approach consisting of first clustering the data, then embedding each cluster, and finally aligning the clusters to obtain a global embedding. We demonstrate this approach on several synthetic and real-world datasets and show that it is competitive with existing methods, while being much more transparent.

## 1 Introduction

Visualization is one of the most commonly used tools in exploratory data analysis (EDA). However, when the data is high-dimensional, direct visualization of the data is not possible and dimensionality reduction techniques must be used to obtain a low-dimensional visualization.

In this paper, we assume the data are of the form  $\{x_i\}_{i=1}^n \subset \mathbb{R}^d$ . We seek an embedding  $\{y_i\}_{i=1}^n \subset \mathbb{R}^m$  with  $m \leq d$  so that if a clustered structure is present in the data, the embedding uncovers the structure and provides visualization of that structure. Typically,  $m = 2$  and we will assume this is the case for the remainder of the paper, though results can easily be extended for  $m > 2$ . As stated, the problem is ill-defined as it is not clear what exactly is to be optimized.

The visualization of clustered data is certainly not a new problem. Early work includes that of Shepard [28], who proposed the practice of imposing the clusters obtained from a hierarchical clustering algorithm onto an embedding. Shepard explains that imposing hierarchical clustering onto the spatial representation provides more information than a hierarchical cluster tree alone (e.g., that two clusters are closer to one another than a third cluster). While his proposal is based on small datasets ( $n = 16$  in his motivating example), the practice of imposing clustering on an embedding is very common. The visualization of single-cell RNA sequencing data in Bioinformatics is a case in point, as data of that sort are typically expected to be clustered [4]. Such data are often visualized by first producing an embedding using, e.g., t-SNE [35] or UMAP [23], and the points are then colored according to known labels or the labeling of some clustering method, e.g., Louvain [3], Leiden [33], or DBSCAN [9]. Similarly, in machine learning in the task of classification, it is common to visualize high-dimensional data such as images or the hidden layers of a neural network with the embedded points colored according to the class label.

Many classical approaches for constructing an embedding seek to preserve some measure of dissimilarity between points, often the Euclidean distance. Examples include classical scaling (CS),

which coincides with principal component analysis (PCA) when the dissimilarity measure is the Euclidean distance; and Isomap [31], which approximates the geodesic distances between points under the assumption that they lie on a smooth submanifold, and then embeds the points using CS with these distances. However, these methods for dimension reduction were not explicitly designed for the visualization of clustered data, and tend not to separate the clusters well. In particular, when embedding a configuration of points in  $\mathbb{R}^d$  into  $\mathbb{R}^2$  or  $\mathbb{R}^3$  there may not be enough space in the low-dimensional embedding space to accommodate all points at a given distance scale. As a result of this “crowding problem” [35], the embedding may collapse distant points together and distinct clusters in the high-dimensional space may overlap in the visualization.

More recently, there has been a class of methods for nonlinear dimensionality reduction that seek to preserve local neighborhoods. Examples include Laplacian eigenmaps [2], as well as the highly popular t-SNE [35] and UMAP [23]. Laplacian eigenmaps is presented as an algorithm that both clusters and embeds the data at the same time [2], as is clear through the strong connection between the method and spectral clustering. However, force-directed methods such as t-SNE and UMAP which aim to balance attractive and repulsive forces between points, are generally recognized as the most successful methods for the visualization of clustered data, in the sense that they tend to separate existing clusters rather well in the embedding. Böhm et al. [4] demonstrates that all three of these methods are closely related, showing that varying the early exaggeration parameter in t-SNE yields a spectrum of embeddings that includes UMAP and Laplacian eigenmaps. In particular, when the t-SNE early exaggeration parameter is small, the resulting visualization contains a more discrete cluster structure and has higher  $k$ -nearest neighbor ( $k$ NN) recall, and when the parameter is larger, attractive forces are increased and the visualization emphasizes more connections between clusters. For another take, Cai and Ma [5] show that during the initial early exaggeration stage of t-SNE,  $\{y_i\}_{i=1}^n$  are clustered according to the cluster membership of  $\{x_i\}_{i=1}^n$ , and during the next stage, the embedding stage, each  $y_i$  is initially updated in a manner determined by a repulsive force from each of the other clusters. Arora et al. [1] and Linderman and Steinerberger [21] provide alternate conditions under which t-SNE will cluster well-separated data so that for each cluster in the original space, there exists a well-separated corresponding cluster in the t-SNE visualization.

However, while these theoretical guarantees on t-SNE lend credibility to it as a method that can separate clusters, we argue that a good visualization method should also preserve some geometrical information, such as the relative position, distances, and sizes of different clusters. Others have similarly advised that despite their popularity in Bioinformatics, t-SNE and UMAP should be used with caution, citing large distortions in distances and global structure [6], as the relative positions and sizes of clusters do not necessarily reflect such information in the original space [39]. Proper PCA initialization of these methods may help mitigate some of these issues [15, 16], but empirically, there remains a trade-off between dimensionality reduction methods that: (i) preserve local structure and separate distinct clusters; and (ii) preserve global distances [4, 7].

Related to our approach is a class of bottom-up manifold learning methods, which start by constructing low-dimensional, low-distortion embeddings of local neighborhoods of the data and then align these local embeddings to produce a single global embedding [8, 17, 18, 41]. However, these methods are not focused on clustered data, and indeed, their global alignment step can result in points from different clusters overlapping in the global embedding.

**Contribution** In this paper, we propose a general framework that aims to strike a compromise between a faithful embedding at the cluster-level and a faithful global embedding of all the data that preserves distances. As explained in [5], t-SNE can be viewed as a method that first clusters the data while embedding it and then aligns the clustered data. We propose an alternate method

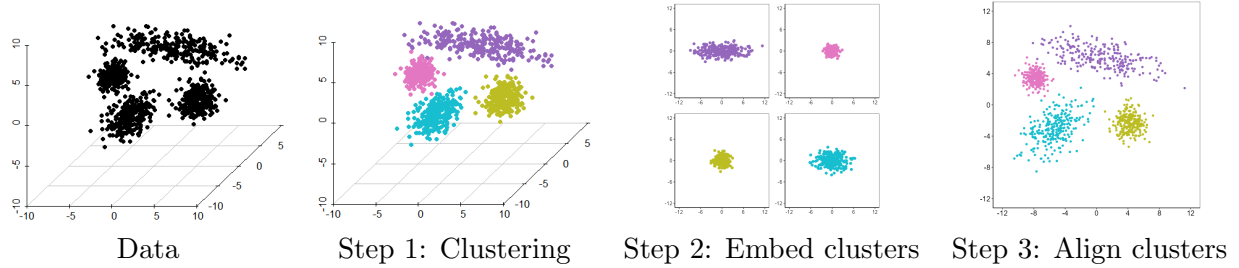


Figure 2.1: Schematic diagram depicting the steps of the Cluster+Embed approach .

that consists of first clustering the data, then embedding each cluster individually, and finally finding rigid transformations to align the clusters in a global embedding so that there is meaningful organization of all clusters together. By embedding each cluster individually, we aim to produce an embedding that suffers from less distortion than if we were to embed all of the data together. Additionally, the method includes a tuning parameter to increase separation between clusters in a way that preserves relative distances between clusters. Our approach is modular in that the clustering and embedding methods may be chosen by the user based on what information they aim to obtain from the visualization. We show that the method is competitive with existing methods, while offering more flexibility and transparency.

*Remark 1.1.* So that there is no confusion, we mention of a very recent article [25], where the authors employ a partition-then-embed strategy (clearly stated in the title of the article), but they partition or group features (i.e., coordinates or dimensions) not observations, and produce an embedding based on each group of features, their intention being the visualization the same data from different ‘perspectives’, as it were.

## 2 The Cluster+Embed approach

Among existing dimensionality reduction methods, there appears to be a trade-off between *(i)* preserving local structure and separate distinct clusters, and *(ii)* preserving global distances. Broadly stated, we study the general approach, which we simply refer to as **Cluster+Embed** (abbreviated *C+E*), that consists in finding an embedding that highlights the cluster structure (when present) with the goal of striking a good balance between *(i)* and *(ii)* above. By first clustering the original data, we aim to preserve the cluster structure in the data, and by embedding each cluster individually, we aim to produce an embedding with less distortion than if we were to embed all of the data together. More concretely, we propose an approach consisting of three steps outlined in Figure 2.1:

1. *Cluster the data.* This can be done using any clustering method the analyst chooses. The intention here is, of course, to reveal any cluster structure in the data.
2. *Embed each cluster separately.* This can be done using any embedding method the analyst chooses. The embedding method is applied to each cluster of points identified in the previous step. The intention here is to obtain a high-quality embedding of each cluster as compared to an embedding of all the data together.
3. *Align the embedded clusters.* The last step consists of aligning the embedded clusters using only rigid transformations. There are multiple ways of doing so and here too, the analyst has a choice. The intention is to obtain an embedding of the entire dataset that preserves

the high-quality embeddings produced in the previous step while also reproducing, as faithfully as possible, the positioning of the clusters with respect to each other. We propose the use of a tuning parameter that controls the separation between clusters, which can then be exaggerated to minimize overlap in order to better visualize the clusters.

The C+E approach is both modular and straightforward, allowing the user the flexibility to produce a visualization for their purpose while being much more transparent in terms of what is being preserved at the cluster level and at the global level compared to other methods such as t-SNE or UMAP that are known to produce clusters when embedding data.

**Notation** We take  $\delta_{ij}$  as a measure of dissimilarity between  $x_i$  and  $x_j$ . For example,  $\delta_{ij}$  could be the Euclidean distance,  $\|x_i - x_j\|$ . The “Swiss roll” is an often used example of the importance of the choice of the dissimilarity measure, where the Euclidean distance between two points does not capture their intrinsic similarity well, and rather the geodesic distance would be a much more appropriate measure of dissimilarity [26, 31]. Another example is the MNIST dataset of handwritten digits in  $\mathbb{R}^{28 \times 28}$ , where Euclidean distance is strongly affected by pixel position (e.g., shifting a digit to the left would result in an image very dissimilar from the original image). For our simplest examples, we set  $\delta_{ij} = \|x_i - x_j\|$  though for some examples where we do not expect the Euclidean distance to capture dissimilarity well, we approximate the geodesic distance from the  $k$ NN graph as in Isomap [31].

## 2.1 Step 1: Cluster the data

For the first step, any clustering method can be used to obtain  $\kappa$  clusters  $\mathcal{C}_1, \dots, \mathcal{C}_\kappa$  which partition  $[n] = \{1, \dots, n\}$ . In Biology, the Louvain and Leiden algorithms are popular choices and tend to work well in practice [3, 33]. DBSCAN and spectral clustering do not make strong assumptions on the clusters and are also effective on a wide variety of datasets [9, 24, 38]. Some methods such as DBSCAN label some points as “noise” not belonging to any cluster. These points could be discarded at this step and excluded from the visualization.

t-SNE (described in Appendix A for the reader’s convenience) is known to produce an embedding in which the data is clustered. Cai and Ma [5] provide some theoretical explanation, establishing that during the early exaggeration stage, t-SNE is approximately performing spectral clustering to both create an embedding and cluster the data. More specifically, during the early exaggeration stage, t-SNE converges to the projection of the initial state onto the null space of the Laplacian of the adjacency matrix with entries  $p_{ij}$  (A.1). If the data is strongly clustered, this representation separates the data into tight clusters. Points in the same cluster will be close to one another, but in this representation the distance between points in the same cluster is not necessarily meaningful, and with random initialization, the relative positions of different clusters is meaningless. Moreover, if the data is only weakly clustered, early stopping of this stage becomes critical to avoid the forming of false clusters.

In contrast, compared to t-SNE, the C+E approach is more explicit and also allows for more direct control of how the clustering is done. For example, Shepard [28] uses some form of hierarchical clustering.

## 2.2 Step 2: Embed each cluster separately

For the second step, any embedding method can be used to separately embed each of the clusters obtained in Step 1. This gives us an embedding  $\{y_i\}_{i=1}^n$ . In general, any method will incur some distortion when embedding high-dimensional data into two dimensions, but by embedding each

cluster individually we can produce an embedding which suffers from less distortion than if we were to embed all of the data together. An added advantage is that, when applying a separation between clusters as described in Step 3, we can more intentionally minimize or even avoid overlap of different clusters.

The choice of embedding method can be guided by what the practitioner hopes to gain from the visualization at the cluster level. If distance preservation is desired, PCA or Isomap may be an appropriate choice. If preservation of local structure is more important, a method that directly aims to embed a local neighborhood graph of the cluster could be used. For example, if the user wants to optimize for  $k$ NN recall for a particular  $k$ , a method for embedding nearest neighbor graphs could be used, e.g., the LOE algorithm proposed by Terada and Von Luxburg [32], which uses a majorization approach to minimizing

$$\sum_{i=1}^n \sum_{j \in \mathcal{N}_i} \sum_{l \notin \mathcal{N}_i} \max (0, \|y_i - y_j\| + \nu - \|y_i - y_l\|)^2,$$

where  $\mathcal{N}_i \subset \{1, \dots, n\}$  indexes the set of  $k$  nearest neighbors of  $x_i$  among  $\{x_j, j \neq i\}$ , and  $\nu$  is a tuning parameter. Practically speaking, we found the gradient descent implementation of LOE by Vankadara et al. [36] converges faster and results in a higher quality embedding as measured by the  $k$ NN recall compared to the majorization approach.

Note that LOE is based only on ordinal information, and so we synchronize the scales of the cluster embeddings before the next step. To do this, when using LOE as the embedding method we propose to scale all  $y_i \in \mathcal{C}_l$  by

$$\gamma_l = \frac{\sum_{i,j \in \mathcal{C}_l} \delta_{ij} \|y_i - y_j\|}{\sum_{i,j \in \mathcal{C}_l} \|y_i - y_j\|^2},$$

where  $\gamma_l$  comes from minimizing the quadratic loss between the embedded distances and original dissimilarities

$$\sum_{i,j \in \mathcal{C}_l} (\gamma_l \|y_j - y_j\| - \delta_{ij})^2.$$

### 2.3 Step 3: Align the embedded clusters

As the final step, we globally align the cluster embeddings using only rigid transformations (translations, reflections, and rotations) so as to position the clusters relative to each other with consideration for their relative positions before embedding, while strictly preserving the pairwise distances within each cluster-level embedding. Our intention is to find some rigid transformations  $T_1, \dots, T_\kappa$  such that

$$\|T_i(y_l) - T_j(y_m)\| \approx \delta_{lm} \quad \text{for all (or most) } l \in \mathcal{C}_i, m \in \mathcal{C}_j, \text{ for all pairs } 1 \leq i < j \leq \kappa. \quad (2.1)$$

That is, we seek rigid transformations that best preserve the pairwise dissimilarities between points in different clusters without updating the cluster-level embeddings. To formalize this, we use a definition of stress, for concreteness Kruskal's definition [19, 20] chosen among others [11, 22, 27, 29], and write (2.1) as an optimization problem

$$\underset{T_1, \dots, T_\kappa \in \mathcal{R}}{\text{minimize}} \quad \sum_{1 \leq i < j \leq \kappa} \sum_{l \in \mathcal{C}_i} \sum_{m \in \mathcal{C}_j} (\delta_{lm} - \|T_i(y_l) - T_j(y_m)\|)^2, \quad (2.2)$$

where  $\mathcal{R}$  is the class of rigid transformations on  $\mathbb{R}^2$ . In this way, we attempt to enforce preservation of distances between points in different clusters, with the constraint that the distances between embedded points in the same cluster cannot be updated to do so.

### 2.3.1 Scaling to avoid cluster overlap

Note that the objective (2.2) does not preclude the possibility of overlap between the embedded clusters, and overlapping clusters may be undesirable when visualization is the end goal. We address this issue by effectively forcing a separation between clusters. The basic idea is to introduce a scaling in (2.1) controlled by a tuning parameter  $\alpha \geq 1$ , specifically

$$\|T_i(y_l) - T_j(y_m)\| \approx \alpha \delta_{lm} \quad \text{for all (or most) } l \in \mathcal{C}_i, m \in \mathcal{C}_j, \text{ for all pairs } 1 \leq i < j \leq \kappa.$$

This uniformly increases the distances between points in different clusters, which encourages separation between the embedded clusters and avoids the crowding problem (see Section 2.3.2). In this case we, the optimization problem (2.2) becomes

$$\underset{T_1, \dots, T_\kappa \in \mathcal{R}}{\text{minimize}} \quad \sum_{1 \leq i < j \leq \kappa} \sum_{l \in \mathcal{C}_i} \sum_{m \in \mathcal{C}_j} (\alpha \delta_{lm} - \|T_i(y_l) - T_j(y_m)\|)^2. \quad (2.3)$$

Numerically, to search over rigid transformations, we use the fact that any rigid transformation of  $\mathbb{R}^2$  is either a rotation followed by translation or a reflection followed by a translation. Thus, we parameterize  $T_i$  by  $(\theta_i, \pi_i, v_i) \in [0, 2\pi) \times \{0, 1\} \times \mathbb{R}^2$ , where

$$T_i(x) = \begin{bmatrix} 1 & 0 \\ 0 & (-1)^{\pi_i} \end{bmatrix} \begin{bmatrix} \cos \theta_i & \sin \theta_i \\ -\sin \theta_i & \cos \theta_i \end{bmatrix} x + v_i.$$

Then the optimization in (2.3) is carried out over  $\{(\theta_i, \pi_i, v_i)\}_{i=1}^\kappa$ . After some initialization, we adopt an alternate minimization going over the  $\kappa \times 3$  parameters in turn, each time with the intention of minimizing the stress (2.3): minimization over  $\theta$  is done by grid search over  $[0, 2\pi)$ ; minimization over  $\pi$  is exhaustive and trivial as it only takes two values; and minimization over  $v$  is done with the use of the BFGS algorithm. In our implementation, we start by embedding the largest cluster, which is then held fixed serving as reference while the other clusters are iteratively positioned.

Compared to t-SNE, which uses attractive and repulsive forces to produce a global embedding that effectively align the clusters (this is done simultaneously in t-SNE), here too the C+E approach is more transparent and more modular, as the analyst is free to align the clusters as they wish. Our choice is based on strictly preserving the cluster embeddings obtained in Step 2.

### 2.3.2 The crowding problem

When embedding high-dimensional data, it is possible there will not be enough space in the low-dimensional embedding space to accommodate all points at a given distance scale. This is referred to as “the crowding problem” by Van der Maaten and Hinton [35].

We illustrate this with an example in Figure 2.2 where we consider a  $d$ -dimensional isotropic Gaussian mixture model (GMM) with  $d$  components where the means of each component have equal pairwise separation and large enough pairwise separation so that the components are well-separated clusters. We take  $d = 10$  in this example. At the far left of Figure 2.2, we observe that PCA on this dataset gives a high amount of overlap between the clusters. Second from left is the result of our method, with clustering via  $k$ -means, embedding each cluster using PCA, and then alignment to optimize (2.2) (or (2.3) with  $\alpha = 1$ ). We observe a moderate amount of overlap between the clusters, which form a ring of radius  $r \approx 4.98$ . However, in a ring of radius  $r$ , there is roughly only room for at most  $2\pi r / \tau$  clusters without overlap, where  $\tau$  is the average diameter of an embedded cluster. In this example, we find  $\tau \approx 4.21$ , so that  $2\pi r / \tau \approx 8$ , and indeed we observe that the clusters overlap.

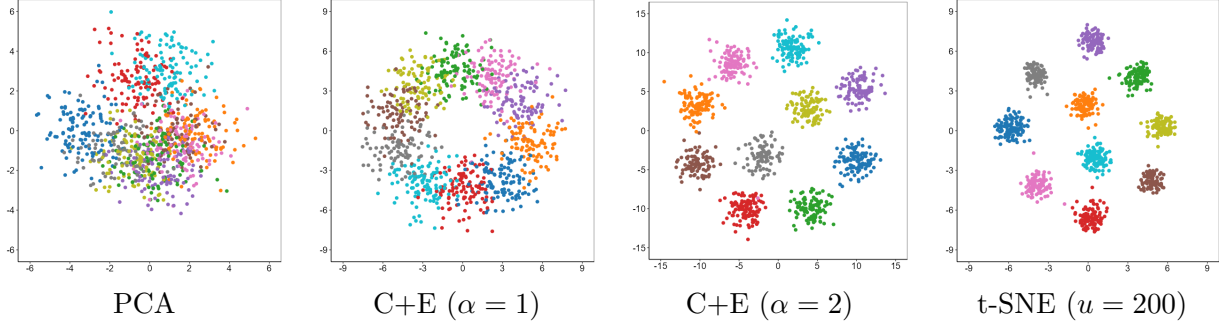


Figure 2.2: Data generated from a 10-dimensional isotropic Gaussian mixture model with equal distance between every pair of clusters. Points are colored by the mixture component they were generated from. These labels were not used by the embedding methods. When  $\alpha = 1$ , C+E produces an embedding with overlapping clusters, whereas  $\alpha = 2$  scales the distances enough to avoid the crowding problem.

Third from the left is the result of our method with  $\alpha = 2$ , which is seen in this example to be enough scaling to avoid almost any overlap. For reference, we also provide on the far right the embedding produced by t-SNE. Qualitatively, both methods produce similar embeddings with clusters in a ring surrounding two clusters in the center. We also note that the relative positioning of clusters in this example is not particularly meaningful, as in the underlying model all clusters have the same distance from one another. Despite the similarity of the embeddings of our method with  $\alpha = 2$  and t-SNE, the crowding problem is addressed differently, and more opaquely by t-SNE, which is based on using the Cauchy kernel, instead of the Gaussian kernel, to model the similarity between points in the embedding. The justification given by Van der Maaten and Hinton [35] for using the Cauchy kernel is that the heavy tails of this kernel “allows a moderate distance in the high-dimensional space to be faithfully modeled by a much larger distance in the map”. See Appendix B for a more quantitative comparison between our method and t-SNE.

In general, a value of  $\alpha$  can be selected in an automatic or data-driven manner by optimizing (over  $\alpha$ ) some criterion of interest, such as the  $k$ NN recall for a particular value of  $k$ . However, this tuning can be computationally expensive and we also suggest an alternative choice which does not require any optimization over  $\alpha$ . The basic idea is that we wish to accommodate  $2\pi r/\tau > \kappa$  clusters within a distance  $r$  from a fixed cluster. Setting  $r = \alpha\Delta$ , where  $\Delta$  is the average distance between two different clusters defined as

$$\Delta = \frac{1}{\kappa \cdot (\kappa - 1)} \sum_{1 \leq i < j \leq \kappa} \sum_{l \in \mathcal{C}_i, m \in \mathcal{C}_j} \Delta_{ij}, \quad \text{with } \Delta_{ij} = \frac{1}{|\mathcal{C}_i|} \frac{1}{|\mathcal{C}_j|} \sum_{l \in \mathcal{C}_i} \sum_{m \in \mathcal{C}_j} \delta_{lm}, \quad (2.4)$$

we solve for  $\alpha$  to obtain

$$\alpha = \max \left( 1, \frac{\kappa\tau}{2\pi\Delta} \right). \quad (2.5)$$

This yields  $\alpha = 1.75$  in the GMM example of Figure 2.2. Again, see Appendix B for a quantitative performance evaluation of this choice of  $\alpha$ .

**Run time** The computational complexity of the method is quadratic in the number of data points, which limits its practicality. One possibility is to subsample the datasets. We found this sufficient to produce useful numerical illustrations and comparisons. Another possibility, which we

leave for future work is to use subsampling to evaluate (2.3)—which is the most computationally-demanding step leading to the quadratic complexity—only considering a random fraction of points from each cluster at each iteration.

### 3 Visualizing Meaningful Clusters

In this section, we demonstrate our method, Cluster+Embed (C+E), on a variety of datasets. We include metrics aimed at evaluating preservation of cluster-level structure in terms of neighborhood recall and distance preservation, as well as metrics aimed at evaluating preservation of global structure in terms of distance preservation and the relative positioning of clusters; see Table 1 for details. Additional experiments are presented in Appendix B. R code to reproduce all figures and results is available at [https://github.com/lizzycoda/cluster\\_embed](https://github.com/lizzycoda/cluster_embed).

Performance metric	Description
$k$ NN recall	The fraction of $k$ -nearest neighbors ( $k$ NN) of a point in the original space that are also $k$ NN in the embedding. We report the average $k$ NN recall over all points for select values of $k$ .
Spearman correlation	Spearman correlation of the pairwise dissimilarities in the original space and the pairwise distances in the embedding. We report the average cluster-wise Spearman correlation and the Spearman correlation for the entire dataset.
Normalized stress	Kruskal's [19, 20] normalized stress over points in each cluster. We report on the average cluster-wise normalized stress and the normalized stress over the entire dataset.
Cluster preservation	Spearman correlation of the distance between clusters in the original space and the embedded space. (We take the distance between a pair of clusters as $\Delta_{ij}$ , defined in (2.4), in the original space, and the analog in the embedded space.)

Table 1: Description of metrics used in evaluation. Here a cluster refers to a ground-truth cluster label rather than ones obtained by a clustering algorithm.

#### 3.1 Example: Shapes I

We begin with a simple example where  $\{x_i\}_{i=1}^n \subset \mathbb{R}^3$  consists of clusters from the DS3 dataset in the R package `dbSCAN` [10] projected onto the surface of a half cylinder. This example is realizable in  $\mathbb{R}^2$ , meaning that there exists  $\{y_i\}_{i=1}^n$  such that  $\|y_i - y_j\| = \delta_{ij}^G$  for all pairs  $(i, j)$ , where  $\delta_{ij}^G$  is the geodesic distance between  $x_i$  and  $x_j$  along the surface of the cylinder. In this case, there is a correct embedding of the data in  $\mathbb{R}^2$  (up to rigid transformations) corresponding to the unrolled cylinder.

To illustrate our C+E approach, we use Euclidean distances to measure dissimilarity, we cluster the data via DBSCAN, and embed each cluster using PCA. Using (2.5) we use  $\alpha = 1$  in the alignment step. Compared to applying PCA to all of the data at once, which approximately projects the data onto to ‘x-z’ plane, applying PCA to each cluster provides a higher quality embedding of each cluster. For t-SNE we use a perplexity value of  $\rho = 230$ , which was selected to maximize the

Spearman correlation between all pairs of the embedded distances and the original distances. The original data, as well as these embeddings are plotted in Figure 3.1.

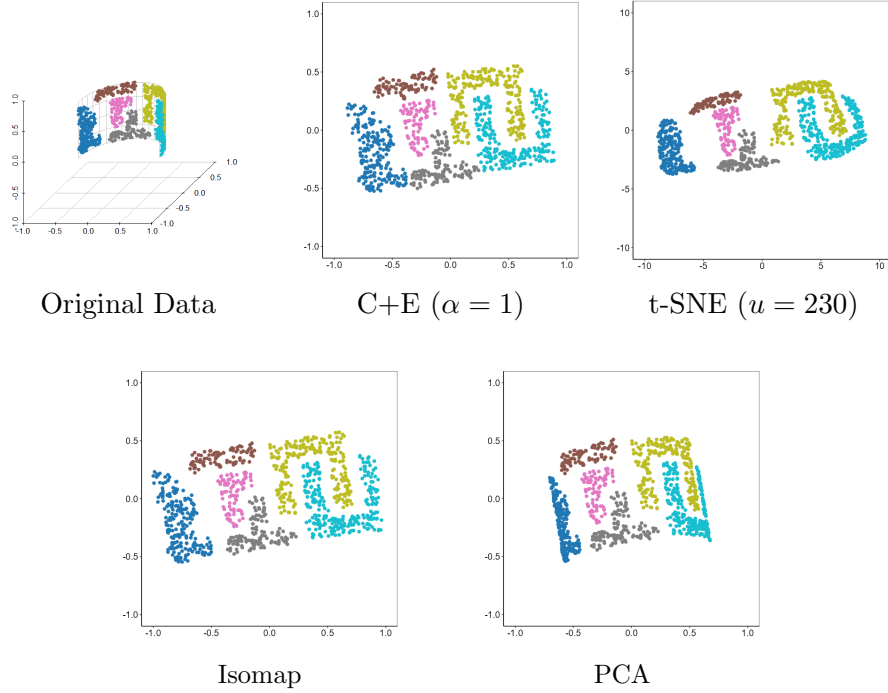


Figure 3.1: Shapes I dataset and embeddings. Points are colored by original cluster label which were not used by either embedding method.

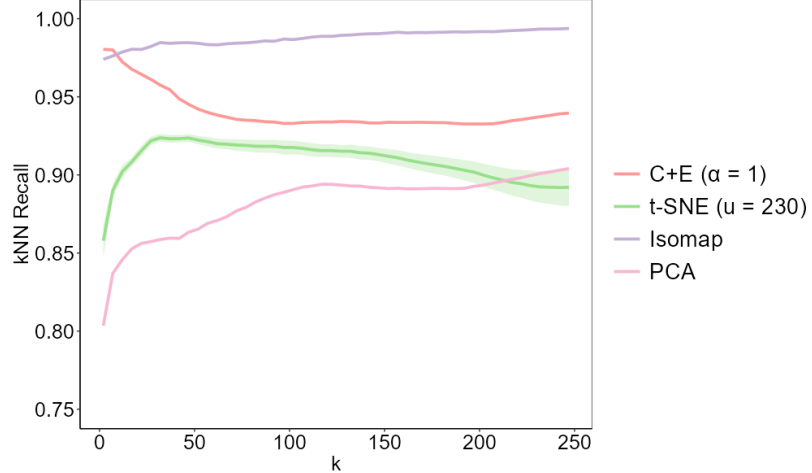


Figure 3.2:  $k$ NN recall for the Shapes I dataset for various values of  $k$  for all methods compared averaged over 5 runs.

We find that while t-SNE clusters the data well and positions the clusters relative to one another reasonably well, the individual clusters are distorted, as well as the overall scale of the embedding. This distortion was present for all perplexity values, and was much higher for values of the perplexity in the typical range suggested in the literature. In contrast, our method recovers

Method	Parameters	Spearman	Normalized Stress
C+E	$\alpha = 1$	$0.998 \pm 0.000$	$0.023 \pm 0.000$
t-SNE	$u = 230$	$0.985 \pm 0.002$	$6.304 \pm 0.238$
Isomap	$q = 400$	<b>1.000</b>	<b>0.015</b>
PCA	-	0.962	0.139

Table 2: Cluster-level metrics for the Shapes I dataset averaged over 5 runs.

Method	Parameters	Spearman	Normalized Stress	Class Preservation
C+E	$\alpha = 1$	$0.993 \pm 0.000$	<b><math>0.086 \pm 0.000</math></b>	$0.967 \pm 0.000$
t-SNE	$u = 230$	$0.949 \pm 0.017$	$9.915 \pm 0.264$	$0.847 \pm 0.036$
Isomap	$q = 400$	<b>0.999</b>	0.148	0.933
PCA	-	0.982	0.105	<b>0.983</b>

Table 3: Global metrics for the Shapes I dataset averaged over 5 runs.

the original point cloud arguably better, both visually and quantitatively as measured by various metrics, both at the cluster level (Table 2) and globally for the entire dataset (Figure 3.2, Table 3). Isomap also performs well on this dataset, in particular on the local metrics.

### 3.2 Example: Shapes II

For our second example, we position  $\{x_i\}_{i=1}^n \subset \mathbb{R}^3$  so that it is not possible to obtain an embedding in  $\mathbb{R}^2$  that preserves all pairwise distances. In this case, there is not a unique, well-defined correct embedding that could serve as reference.

For our method, we use the same combination of DBSCAN and PCA. In Figure 3.3, we include the results of our method using  $\alpha = 1$  and the value of  $\alpha = 1.42$  obtained using (2.5). We also include t-SNE with perplexity  $u = 260$ , chosen to optimize the global Spearman correlation, and with  $u = 50$ , which we found to visually give a better embedding. Note that all metrics but the  $k$ NN recall for small values of  $k$  (Figure 3.4), suggest that t-SNE with  $u = 260$  is a more faithful visualization than t-SNE with  $u = 50$ , even though at the cluster level it appears to suffer from more distortion. In Table 4, we see that the normalized stress at the cluster level is zero with our method, as PCA applied to each cluster individually exactly recovers the configuration of each cluster, each cluster being flat in this example. The alignment step also orients the clusters consistently with their orientation and their positioning in the original space. Cluster-level and global performance metrics are reported in Table 4 and Table 5, respectively.

### 3.3 Example: MNIST

For our first real-world example we test our method on 5000 random examples from the MNIST dataset. For the C+E approach, we set  $\delta_{ij}$  to the geodesic distances approximated from the 5-NN graph, rather than Euclidean distances between images. We also found Wasserstein distances effective on a smaller subset of the dataset, but found these distances were too computationally expensive to compute for 5000 images. We cluster the data via the Leiden algorithm with parameters set to obtain ten clusters. The clustering has a Rand index of 0.924 with the digit labels. The clusters roughly correspond to the digits, with the exception of the ‘fours’ and ‘nines’ being grouped together into one cluster, the ‘ones’ being divided into two clusters, and the ‘fives’ being

divided into two clusters, one of which also contains most of the ‘threes’. In comparison, running  $k$ -Means on the t-SNE ( $u = 20$ ) visualization gave a Rand index of 0.930 with the digit labels. We include results for two embedding methods, Isomap ( $q = 5$ ) and LOE ( $k = 10, \nu = 10^{-6}$ ) and depict the results in Figure 3.5.

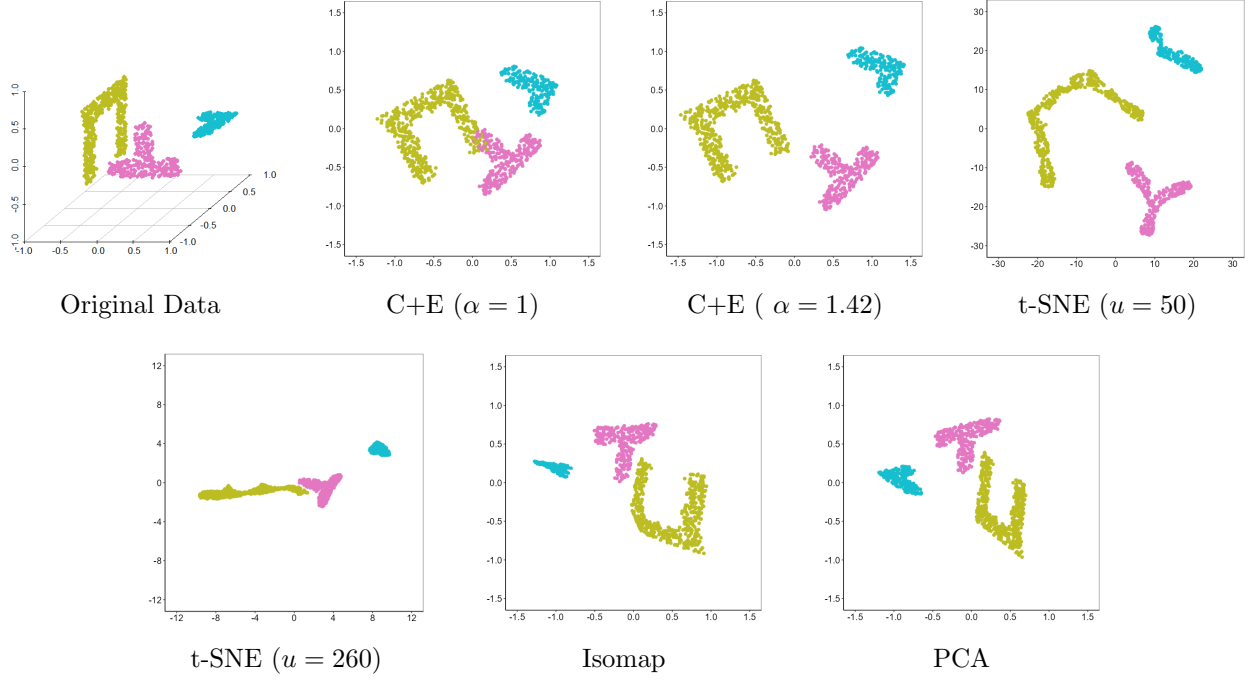


Figure 3.3: Shapes II dataset and embeddings. Points are colored by original cluster label which were not used by either embedding method.

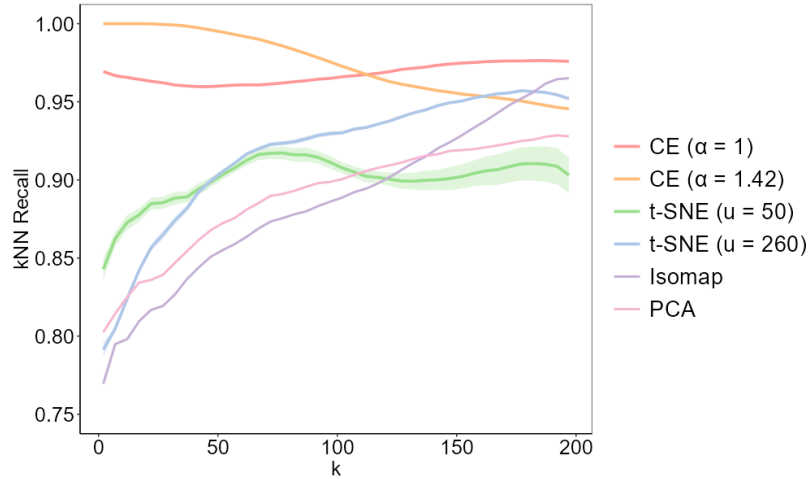


Figure 3.4:  $k$ NN recall for the Shapes II dataset for various values of  $k$  for all methods compared averaged over 5 runs.

Method	Parameters	Spearman	Normalized Stress
C+E	$\alpha = 1$	<b><math>1.000 \pm 0.000</math></b>	<b><math>0.000 \pm 0.000</math></b>
C+E	$\alpha = 1.42$	<b><math>1.000 \pm 0.000</math></b>	<b><math>0.000 \pm 0.000</math></b>
t-SNE	$u = 50$	$0.943 \pm 0.004$	$22.895 \pm 0.890$
t-SNE	$u = 260$	$0.954 \pm 0.001$	$3.721 \pm 0.055$
Isomap	$q = 500$	0.828	0.297
PCA	-	0.921	0.285

Table 4: Cluster-level metrics for the Shapes II dataset averaged over 5 runs.

Method	Parameters	Spearman	Normalized Stress	Class Preservation
C+E	$\alpha = 1$	$0.982 \pm 0.000$	<b><math>0.094 \pm 0.000</math></b>	<b><math>1.000 \pm 0.000</math></b>
C+E	$\alpha = 1.42$	$0.976 \pm 0.000$	$0.394 \pm 0.000$	<b><math>1.000 \pm 0.000</math></b>
t-SNE	$u = 50$	$0.783 \pm 0.069$	$24.746 \pm 0.933$	$0.733 \pm 0.596$
t-SNE	$u = 260$	$0.923 \pm 0.002$	$7.438 \pm 0.165$	<b><math>1.000 \pm 0.000</math></b>
Isomap	$q = 500$	<b>0.990</b>	0.117	<b>1.000</b>
PCA	-	0.979	0.124	<b>1.000</b>

Table 5: Global metrics for the Shapes II dataset averaged over 5 runs.

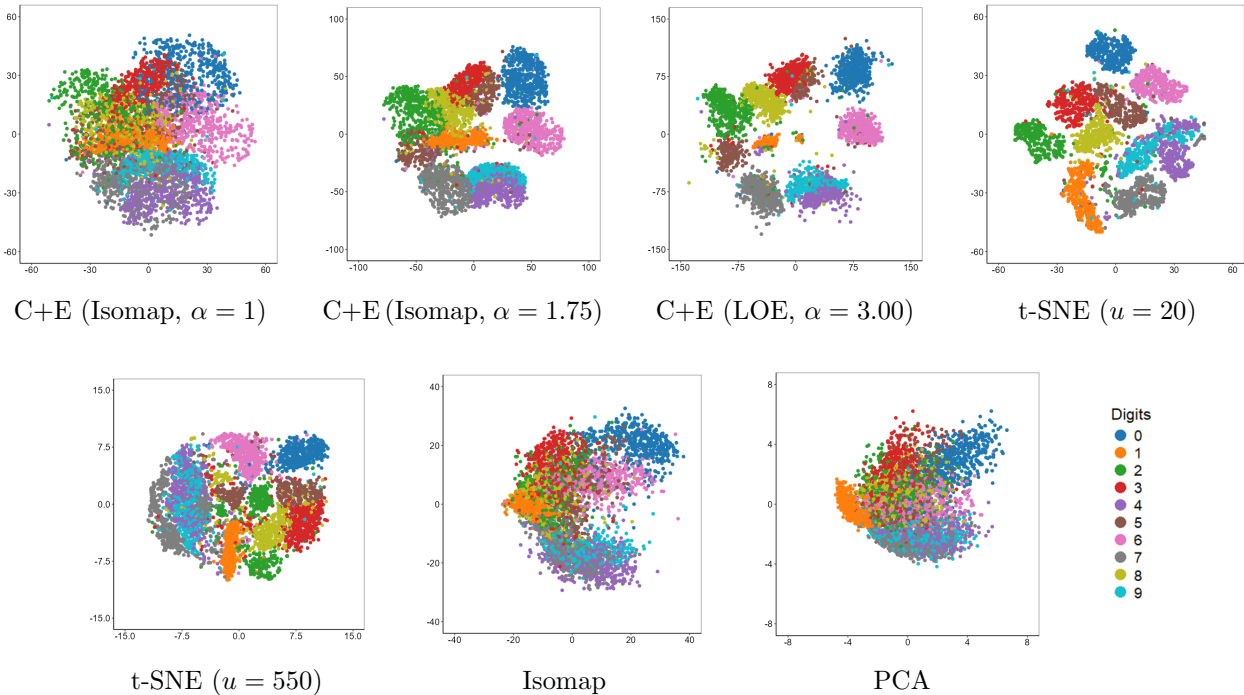


Figure 3.5: Embedding of MNIST dataset. Points are colored according to their original digit label. These labels were not used by the embedding methods.

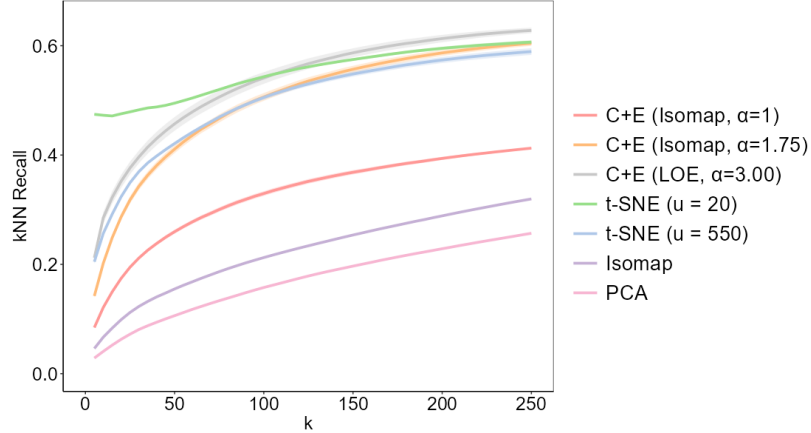


Figure 3.6:  $k$ NN recall for the MNIST dataset for various values of  $k$  for all methods compared averaged over 5 runs.

Method	Parameters	Spearman	Normalized Stress
C+E (Isomap)	$\alpha = 1$	<b><math>0.817 \pm 0.010</math></b>	<b><math>0.322 \pm 0.010</math></b>
C+E (Isomap)	$\alpha = 1.75$	$0.799 \pm 0.010$	$0.499 \pm 0.043$
C+E (LOE)	$\alpha = 3$	$0.753 \pm 0.013$	$1.060 \pm 0.048$
t-SNE	$u = 20$	$0.771 \pm 0.004$	$0.517 \pm 0.004$
t-SNE	$u = 550$	$0.757 \pm 0.009$	$0.825 \pm 0.005$
Isomap	$q = 5$	$0.554$	$0.607$
PCA	-	$0.401$	$0.921$

Table 6: Cluster-level metrics for the MNIST dataset averaged over 5 runs.

Method	Parameters	Spearman	Normalized Stress	Class Preservation
C+E (Isomap)	$\alpha = 1$	$0.660 \pm 0.010$	<b><math>0.342 \pm 0.002</math></b>	<b><math>0.756 \pm 0.021</math></b>
C+E (Isomap)	$\alpha = 1.75$	$0.610 \pm 0.045$	$0.781 \pm 0.005$	$0.618 \pm 0.148$
C+E (LOE)	$\alpha = 3$	$0.601 \pm 0.017$	$1.880 \pm 0.002$	$0.697 \pm 0.051$
t-SNE	$u = 20$	$0.519 \pm 0.051$	$0.397 \pm 0.015$	$0.597 \pm 0.062$
t-SNE	$u = 550$	$0.626 \pm 0.029$	$0.749 \pm 0.005$	$0.657 \pm 0.072$
Isomap	$q = 5$	<b><math>0.680</math></b>	$0.474$	$0.755$
PCA	-	$0.463$	$0.906$	$0.475$

Table 7: Global metrics for the MNIST dataset averaged over 5 runs.

Qualitatively, we find that the arrangement of the clusters by the C+E approach is similar to the arrangement of clusters found by t-SNE. Isomap and PCA applied to all of the data find a similar arrangement of clusters, but fail to separate the clusters. Locally, in Table 6 we find that C+E (Isomap,  $\alpha = 1.75$ ) is comparable to t-SNE ( $u = 20$ ) and globally, in Table 7, it is comparable to t-SNE ( $u = 550$ ). We selected  $u = 550$  to optimize for global Spearman correlation, and also include  $u = 20$  for a representative of t-SNE that achieves better local performance.

In Figure 3.6, we find that for small values of  $k$ , the  $k$ NN recall performance of t-SNE ( $u = 20$ ) is far superior to any other method. We attempt to improve the  $k$ NN recall performance of C+E by embedding via LOE, and in the plot we observe that this improves the  $k$ NN recall performance and surpasses t-SNE for  $k \gtrsim 100$ , however there is still a large gap in performance for small  $k$ .

### 3.4 Example: Single-cell data

As another real-world example, we sample 5000 examples from the developmental human brain organoid data from Kanton et al. [14]. This dataset has been used in other papers that explore t-SNE, including [4, 7] and we use the same preprocessing of the data. For the C+E approach, we again set  $\delta_{ij}$  to the geodesic distances approximated from the 5-NN graph, rather than use Euclidean distances for the embedding. We cluster the data via the Leiden algorithm and obtain nine clusters, which we embed using both Isomap and LOE ( $k = 10, \nu = 10^{-6}$ ) in Figure 3.7.

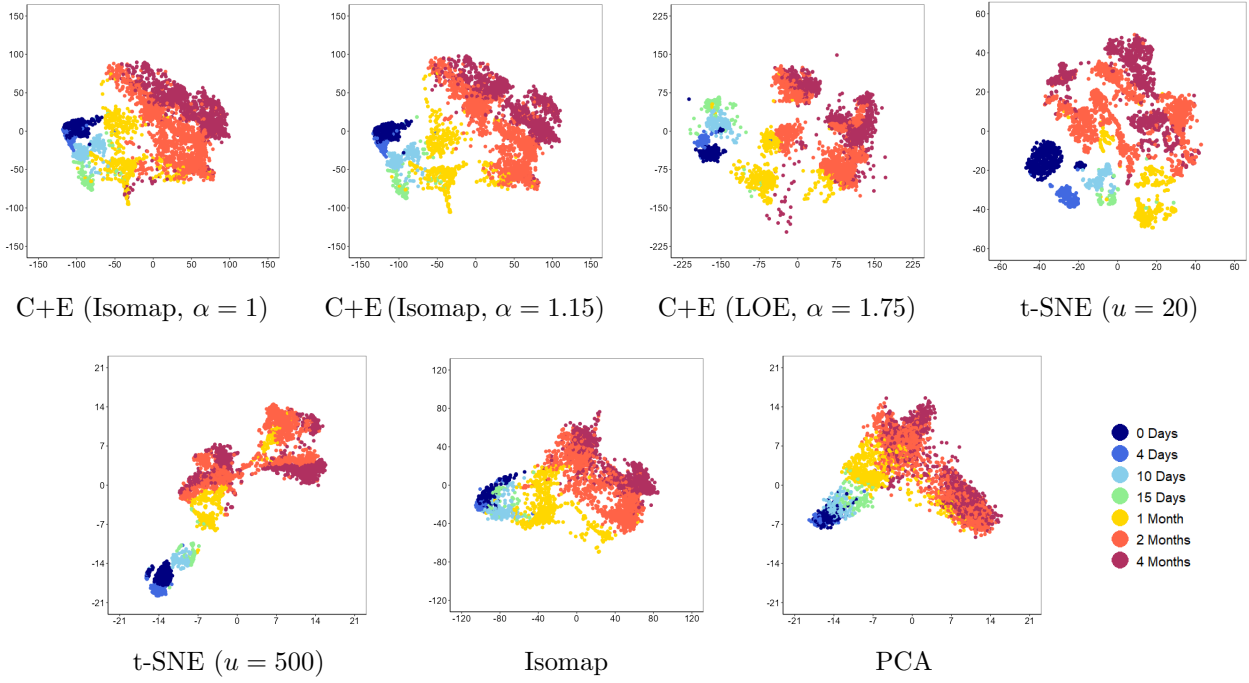


Figure 3.7: Embedding of the human brain organoid dataset. Points are colored by the time points they were sampled at. These labels were not used by the embedding methods.

Visually, both C+E and t-SNE find similar clusters and similar arrangements of the clusters. This is reflected in Table 8 and Table 9 where the Spearman correlations of distances and class preservation metrics are similar between the methods, with the exception of t-SNE with  $u = 20$  which has worse performance on these metrics. We also note that the normalized stress of C+E is better than t-SNE. On the other hand, t-SNE with  $u = 20$  achieves much higher  $k$ NN recall in Figure 3.8 than any other embedding for small  $k$ . The  $k$ NN recall of C+E (LOE) is comparable

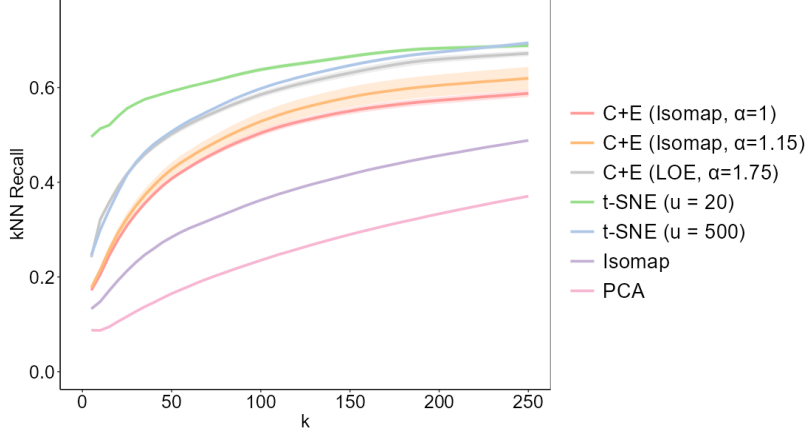


Figure 3.8:  $k$ NN recall for the Human Brain dataset for various values of  $k$  for all methods compared averaged over 5 runs.

Method	Parameters	Spearman	Normalized Stress
C+E (Isomap)	$\alpha = 1$	$0.809 \pm 0.010$	<b><math>0.356 \pm 0.015</math></b>
C+E (Isomap)	$\alpha = 1.15$	$0.817 \pm 0.010$	$0.365 \pm 0.010$
C+E (LOE)	$\alpha = 1.75$	$0.807 \pm 0.013$	$0.666 \pm 0.054$
t-SNE	$u = 20$	$0.789 \pm 0.029$	$0.613 \pm 0.021$
t-SNE	$u = 500$	<b><math>0.825 \pm 0.008</math></b>	$0.895 \pm 0.003$
Isomap	$q = 5$	$0.742$	$0.467$
PCA	-	$0.589$	$0.895$

Table 8: Local metrics for the Human Brain dataset averaged over 5 runs.

Method	Parameters	Spearman	Normalized Stress	Class Preservation
C+E (Isomap)	$\alpha = 1$	$0.896 \pm 0.003$	<b><math>0.210 \pm 0.001</math></b>	$0.910 \pm 0.023$
C+E (Isomap)	$\alpha = 1.15$	$0.903 \pm 0.004$	$0.258 \pm 0.004$	<b><math>0.928 \pm 0.031</math></b>
C+E (LOE)	$\alpha = 1.75$	$0.883 \pm 0.015$	$0.765 \pm 0.002$	$0.905 \pm 0.035$
t-SNE	$u = 20$	$0.628 \pm 0.051$	$0.594 \pm 0.002$	$0.833 \pm 0.113$
t-SNE	$u = 500$	$0.875 \pm 0.002$	$0.821 \pm 0.007$	$0.927 \pm 0.000$
Isomap	$q = 5$	<b><math>0.939</math></b>	$0.243$	$0.918$
PCA	-	$0.852$	$0.848$	$0.910$

Table 9: Global metrics for the Human Brain dataset averaged over 5 runs.

to t-SNE with  $u = 500$ . Isomap and PCA also arrange the clusters similarly to C+E and t-SNE, though PCA does not separate the two and four month cells well. The local metrics of these methods are poor, though Isomap has high global metrics.

## 4 Discussion

Throughout the examples, we observed that no single method dominated the other methods over all of the metrics, even restricting to just the local or global scale. Given these trade-offs between the

different metrics and different embedding methods, we encourage the practitioner to consider what information they wish to obtain from a visualization when choosing an embedding method. The presented C+E approach allows the user the transparency and flexibility to more directly control what the embedding methods emphasizes.

We showed on some toy examples that the C+E approach can better preserve the geometry on the cluster level than t-SNE. On the real-world examples, we demonstrated that C+E with  $\alpha$  large enough for cluster separation was typically comparable to the best performing t-SNE embedding at the local level, and the best performing t-SNE embedding at the global level. The exception to the comparable performance between C+E and t-SNE was on  $k$ NN recall, where t-SNE with small perplexity achieved superior performance for small  $k$ , though this embedding typically underperformed the other embeddings on most other metrics.

The exceptional performance of t-SNE on  $k$ NN recall on the real world datasets compared to other embedding methods such as LOE that embed nearest neighbors graphs is somewhat of a mystery to us. Previous works have argued that t-SNE optimizes the  $k$ NN recall [13, 37], though we find that the argument strays from t-SNE as originally formulated, and assumes a simplified setting where  $q_{ij}$  in (A.2) takes on a binary form. This is exemplified by simply running t-SNE on data in  $\mathbb{R}^2$  with initialization as is, so that the  $k$ NN recall is = 1 for all  $k$  at initialization. We find that t-SNE updates the points in a way that decreases the  $k$ NN recall. In contrast, with a small enough  $\nu$ , LOE achieves perfect  $k$ NN recall in this simple setting. We also note that we can significantly improve the  $k$ NN recall of the C+E approach with LOE embeddings to a level comparable with t-SNE on MNIST and the single-cell dataset if we break the data up into more clusters ( $\approx 25$  clusters) at the clustering step, though this creates the presence of false clusters in the visualization. This approach of breaking up the data into clusters that are not necessarily meaningful appears to somewhat mimic how t-SNE appears to break the data up into small patches and arrange these patches when the perplexity is small even when the data is not clustered, though we leave further investigation of this to future work. This remains a limitation of the proposed method and if the user wishes to obtain a visualization with high  $k$ NN recall, t-SNE may still be the state of the art.

Nonetheless, high  $k$ NN recall is only one of many potentially desirable properties for the visualization of data. With that in mind, our method is competitive and allows for more directly controllable and interpretable visualizations.

## Acknowledgments

We would like to thank Amelia Kawasaki and Tianyao Xu for their initial contributions during early stages of this work. We would also like to thank Eran Mukamel and Elizabeth Purdom for helpful discussions.

## References

- [1] Arora, S., W. Hu, and P. K. Kothari (2018). An analysis of the t-SNE algorithm for data visualization. In *Conference on Learning Theory*, pp. 1455–1462. PMLR.
- [2] Belkin, M. and P. Niyogi (2003). Laplacian eigenmaps for dimensionality reduction and data representation. *Neural Computation* 15(6), 1373–1396.
- [3] Blondel, V. D., J.-L. Guillaume, R. Lambiotte, and E. Lefebvre (2008). Fast unfolding of communities in large networks. *Journal of Statistical Mechanics: Theory and Experiment* 2008(10).
- [4] Böhm, J. N., P. Berens, and D. Kobak (2022). Attraction-repulsion spectrum in neighbor embeddings. *Journal of Machine Learning Research* 23(95), 1–32.

- [5] Cai, T. T. and R. Ma (2022). Theoretical foundations of t-SNE for visualizing high-dimensional clustered data. *Journal of Machine Learning Research* 23(301), 1–54.
- [6] Chari, T. and L. Pachter (2023). The specious art of single-cell genomics. *PLOS Computational Biology* 19, 1–20.
- [7] Damrich, S., M. V. Klockow, P. Berens, F. A. Hamprecht, and D. Kobak (2024). Visualizing single-cell data with the neighbor embedding spectrum. *bioRxiv*.
- [8] Donoho, D. L. and C. Grimes (2003). Hessian eigenmaps: locally linear embedding techniques for high-dimensional data. *Proceedings of the National Academy of Sciences* 100(10), 5591–5596.
- [9] Ester, M., H.-P. Kriegel, J. Sander, and X. Xu (1996). A density-based algorithm for discovering clusters in large spatial databases with noise. In *International Conference on Knowledge Discovery and Data Mining*, pp. 226–231.
- [10] Hahsler, M., M. Piekenbrock, and D. Doran (2019). DBSCAN: Fast density-based clustering with R. *Journal of Statistical Software* 91, 1–30.
- [11] Heiser, W. J. (1988). Multidimensional scaling with least absolute residuals. *Classification and Related Methods of Data Analysis*, 455–462.
- [12] Hinton, G. E. and S. Roweis (2002). Stochastic neighbor embedding. *Advances in Neural Information Processing Systems* 15.
- [13] Im, D. J., N. Verma, and K. Branson (2018). Stochastic neighbor embedding under f-divergences. *arXiv preprint arXiv:1811.01247*.
- [14] Kanton, S., M. J. Boyle, Z. He, M. Santel, A. Weigert, F. Sanchís-Calleja, P. Guijarro, L. Sidow, J. S. Fleck, D. Han, et al. (2019). Organoid single-cell genomic atlas uncovers human-specific features of brain development. *Nature* 574(7778), 418–422.
- [15] Kobak, D. and P. Berens (2019). The art of using t-SNE for single-cell transcriptomics. *Nature Communications* 10(1).
- [16] Kobak, D. and G. C. Linderman (2021). Initialization is critical for preserving global data structure in both t-SNE and UMAP. *Nature Biotechnology* 39(2).
- [17] Kohli, D., A. Cloninger, and G. Mishne (2021). LDLE: Low distortion local eigenmaps. *Journal of Machine Learning Research* 22.
- [18] Kohli, D., J. S. Nieuwenhuis, A. Cloninger, G. Mishne, and D. Narain (2024). Rats: Unsupervised manifold learning using low-distortion alignment of tangent spaces. *bioRxiv*, 2024–10.
- [19] Kruskal, J. B. (1964a). Multidimensional scaling by optimizing goodness of fit to a nonmetric hypothesis. *Psychometrika* 29(1), 1–27.
- [20] Kruskal, J. B. (1964b). Nonmetric multidimensional scaling: a numerical method. *Psychometrika* 29(2), 115–129.
- [21] Linderman, G. C. and S. Steinerberger (2019). Clustering with t-SNE, provably. *SIAM Journal on Mathematics of Data Science* 1(2), 313–332.
- [22] McGee, V. E. (1966). The multidimensional analysis of ‘elastic’ distances. *British Journal of Mathematical and Statistical Psychology* 19(2), 181–196.
- [23] McInnes, L., J. Healy, and J. Melville (2018). UMAP: Uniform manifold approximation and projection for dimension reduction. *arXiv preprint arXiv:1802.03426*.
- [24] Ng, A., M. Jordan, and Y. Weiss (2001). On spectral clustering: Analysis and an algorithm. *Advances in Neural Information Processing Systems* 14.
- [25] Peterfreund, E., O. Lindenbaum, Y. Kluger, and B. Landa (2025). Partition first, embed later: Laplacian-based feature partitioning for refined embedding and visualization of high-dimensional data. *Forty-Second International Conference on Machine Learning*.
- [26] Roweis, S. T. and L. K. Saul (2000). Nonlinear dimensionality reduction by locally linear embedding. *Science* 290(5500), 2323–2326.
- [27] Sammon, J. W. (2006). A nonlinear mapping for data structure analysis. *IEEE Transactions on Computers* 100(5), 401–409.
- [28] Shepard, R. (1972). Psychological representation of speech sounds. *Human Communication: A Unified View*, 67–113.
- [29] Takane, Y., F. W. Young, and J. De Leeuw (1977). Nonmetric individual differences multidimensional scaling: An alternating least squares method with optimal scaling features. *Psychometrika* 42(1), 7–67.
- [30] Tasic, B., Z. Yao, L. T. Graybuck, K. A. Smith, T. N. Nguyen, D. Bertagnolli, J. Goldy, E. Garren,

M. N. Economo, S. Viswanathan, et al. (2018). Shared and distinct transcriptomic cell types across neocortical areas. *Nature* 563(7729), 72–78.

[31] Tenenbaum, J. B., V. d. Silva, and J. C. Langford (2000). A global geometric framework for nonlinear dimensionality reduction. *Science* 290(5500), 2319–2323.

[32] Terada, Y. and U. Von Luxburg (2014). Local ordinal embedding. In *International Conference on Machine Learning*, pp. 847–855. PMLR.

[33] Traag, V. A., L. Waltman, and N. J. Van Eck (2019). From Louvain to Leiden: guaranteeing well-connected communities. *Scientific Reports* 9(1), 1–12.

[34] Van Der Maaten, L. (2014). Accelerating t-SNE using tree-based algorithms. *The Journal of Machine Learning Research* 15(1), 3221–3245.

[35] Van der Maaten, L. and G. Hinton (2008). Visualizing data using t-SNE. *Journal of Machine Learning Research* 9(11).

[36] Vankadara, L. C., M. Lohaus, S. Haghiri, F. U. Wahab, and U. Von Luxburg (2023). Insights into ordinal embedding algorithms: A systematic evaluation. *Journal of Machine Learning Research* 24(191), 1–83.

[37] Venna, J., J. Peltonen, K. Nybo, H. Aidos, and S. Kaski (2010). Information retrieval perspective to nonlinear dimensionality reduction for data visualization. *Journal of Machine Learning Research* 11(2).

[38] Von Luxburg, U. (2007). A tutorial on spectral clustering. *Statistics and Computing* 17, 395–416.

[39] Wattenberg, M., F. Viégas, and I. Johnson (2016). How to use t-SNE effectively. *Distill* 1(10).

[40] Xiao, H., K. Rasul, and R. Vollgraf (2017). Fashion-mnist: a novel image dataset for benchmarking machine learning algorithms. *arXiv preprint arXiv:1708.07747*.

[41] Zhang, Z. and H. Zha (2004). Principal manifolds and nonlinear dimensionality reduction via tangent space alignment. *SIAM Journal on Scientific Computing* 26(1), 313–338.

## A A description of t-SNE

For each pair of points  $x_i$  and  $x_j$ , t-SNE first computes the normalized affinities

$$p_{ij} = \frac{p_{i|j} + p_{j|i}}{2n} \quad \text{where} \quad p_{j|i} = \frac{K(\|x_i - x_j\|/\sigma_i)}{\sum_{k \neq i} K(\|x_i - x_k\|/\sigma_i)}, \quad (\text{A.1})$$

where  $K$  is the Gaussian kernel,  $K(t) = e^{-t^2/2}$ , and  $\sigma_i$  is chosen according to the perplexity parameter  $u$ , so that

$$2^{\mathcal{H}(p_{|i})} = u, \quad \forall i = 1, \dots, n,$$

where  $\mathcal{H}(p_{|i}) = -\sum_j p_{j|i} \log_2 p_{j|i}$  is the entropy. The perplexity can be thought of as controlling the neighborhood size considered in computing the affinities. Most implementations of t-SNE utilize the Barnes-Hut variant of t-SNE [34] which sets  $p_{j|i} = 0$  if  $j$  is not in the  $\lfloor 3u \rfloor$  nearest neighbors of  $x_i$ . The perplexity is typically set in the range of  $5 \leq u \leq 50$  [35].

The t-SNE algorithm, introduced by Van der Maaten and Hinton [35] as a variant of the SNE algorithm proposed earlier by Hinton and Roweis [12], aims to find  $(y_i)_{i=1}^n$  in  $\mathbb{R}^2$  that minimizes the KL divergence

$$\sum_{i \neq j} p_{ij} \log \left( \frac{p_{ij}}{q_{ij}} \right), \quad (\text{A.2})$$

where  $q_{ij}$  is the normalized similarity between  $y_i$  and  $y_j$  computed using the Cauchy kernel  $L(t) = (1+t^2)^{-1}$ ,

$$q_{ij} = \frac{L(\|y_i - y_j\|)}{\sum_{l \neq m} L(\|y_l - y_m\|)}.$$

In practice, the KL divergence (A.2) is minimized using gradient descent with a momentum term. An initial early exaggeration stage is also used during which the  $p_{ij}$  in (A.2) are replaced with  $\rho p_{ij}$  for the first few iterations of gradient descent, with  $\rho > 0$  being a tuning parameter.

## B Complete Results

**GMM** In Section 2.3.2, we depict a  $d$ -dimensional isotropic Gaussian mixture model (GMM) with  $d$  components. Specifically, the mean vector of each component is  $\frac{3}{2}\sqrt{d}e_i$  where the  $i$ th coordinate of  $e_i$  is one and zero otherwise, and we set  $d = 10$ . The complete metrics and additional figures on this example follow.

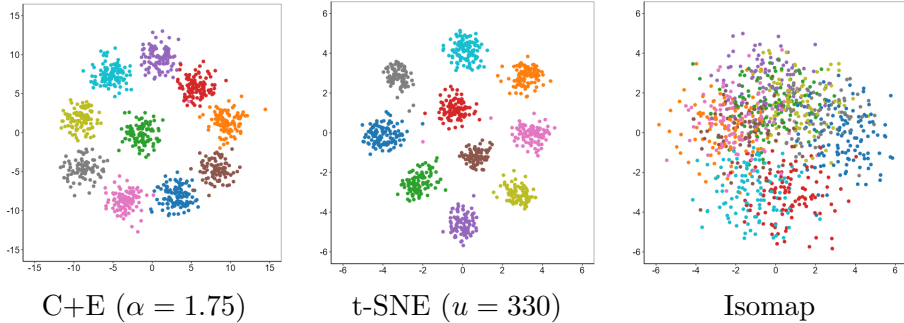


Figure B.1: Data generated from a 10-dimensional isotropic Gaussian mixture model. Points are colored by the mixture component they were generated from. These labels were not used by the embedding methods.

Note that the class preservation metric is not particularly meaningful in this example because in the underlying model, the distance is the same between every pair of clusters. In other words, if in the original sample, cluster  $i$  is closer to cluster  $j$  than cluster  $\kappa$ , this is an artifact of the sample.

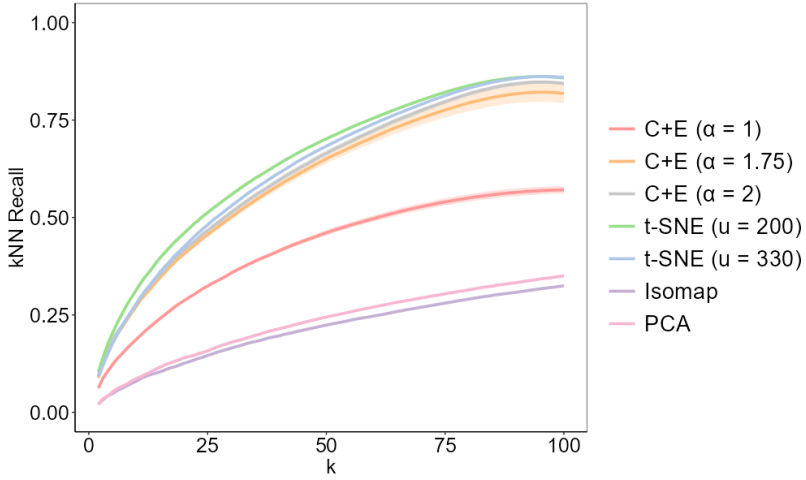


Figure B.2:  $k$ NN recall for the GMM dataset for various values of  $k$  for all methods compared averaged over 5 runs.

Method	Parameters	Spearman	Normalized Stress
C+E	$\alpha = 1$	$0.542 \pm 0.017$	<b><math>0.536 \pm 0.003</math></b>
C+E	$\alpha = 1.75$	$0.528 \pm 0.018$	$0.558 \pm 0.020$
C+E	$\alpha = 2$	$0.536 \pm 0.021$	$0.545 \pm 0.012$
t-SNE	$u = 200$	<b><math>0.641 \pm 0.005</math></b>	$0.779 \pm 0.007$
t-SNE	$u = 330$	$0.587 \pm 0.005$	$0.830 \pm 0.006$
Isomap	$q = 500$	0.414	0.541
PCA	-	0.415	0.609

Table 10: Cluster-level metrics for the GMM dataset averaged over 5 runs.

Method	Parameters	Spearman	Normalized Stress	Class Preservation
C+E	$\alpha = 1$	$0.386 \pm 0.015$	<b><math>0.378 \pm 0.003</math></b>	$0.057 \pm 0.233$
C+E	$\alpha = 1.75$	$0.354 \pm 0.012$	$0.785 \pm 0.002$	$0.123 \pm 0.164$
C+E	$\alpha = 2$	$0.337 \pm 0.013$	$0.992 \pm 0.001$	$0.053 \pm 0.150$
t-SNE	$u = 200$	$0.377 \pm 0.008$	$0.388 \pm 0.006$	$0.200 \pm 0.151$
t-SNE	$u = 330$	$0.412 \pm 0.008$	$0.458 \pm 0.007$	$0.343 \pm 0.144$
Isomap	$q = 500$	0.440	0.532	0.517
PCA	-	<b>0.443</b>	0.581	<b>0.470</b>

Table 11: Global metrics for the GMM dataset averaged over 5 runs.

**MNIST** In the main text, we evaluated each embedding compared to the dissimilarities  $\delta_{ij}$  in the original space, the geodesic distances approximated from the 5-NN graph. C+E is directly given these dissimilarities as input whereas t-SNE is only given  $\{x_i\}_{i=1}^n$  as input. To be fair, we also evaluate each embedding against the Euclidean distances in the original space. At both the cluster-level and global level, t-SNE has a smaller normalized stress than C+E, but all other metrics remain comparable (with C+E superior in terms of class preservation).

Method	Parameters	Spearman	Normalized Stress
C+E (Isomap)	$\alpha = 1$	<b>0.691 ± 0.008</b>	$1.779 \pm 0.032$
C+E (Isomap)	$\alpha = 1.75$	$0.661 \pm 0.009$	$2.670 \pm 0.094$
C+E (LOE)	$\alpha = 3.00$	$0.621 \pm 0.014$	$4.580 \pm 0.135$
t-SNE	$u = 20$	$0.651 \pm 0.008$	$1.304 \pm 0.049$
t-SNE	$u = 550$	$0.687 \pm 0.009$	<b>0.569 ± 0.008</b>
Isomap	$q = 5$	0.513	0.758
PCA	-	0.479	0.756

Table 12: Cluster-level metrics on the MNIST dataset averaged over 5 runs using Euclidean distance to measure pairwise dissimilarity of the original data.

Method	Parameters	Spearman	Normalized Stress	Class Preservation
C+E (Isomap)	$\alpha = 1$	$0.518 \pm 0.004$	$2.979 \pm 0.000$	<b>0.578 ± 0.026</b>
C+E (Isomap)	$\alpha = 1.75$	$0.473 \pm 0.021$	$5.700 \pm 0.038$	$0.500 \pm 0.092$
C+E (LOE)	$\alpha = 3.00$	$0.447 \pm 0.015$	$10.300 \pm 0.018$	$0.502 \pm 0.062$
t-SNE	$u = 20$	$0.363 \pm 0.072$	$3.514 \pm 0.076$	$0.409 \pm 0.088$
t-SNE	$u = 550$	$0.518 \pm 0.023$	<b>0.433 ± 0.018</b>	$0.452 \pm 0.060$
Isomap	$q = 5$	<b>0.540</b>	1.649	0.475
PCA	-	0.524	0.642	0.332

Table 13: Global metrics on the MNIST dataset averaged over 5 runs using Euclidean distance to measure pairwise dissimilarity of the original data

**Single-cell data** In the main text, we evaluated each embedding compared to the dissimilarities  $\delta_{ij}$  in the original space, the geodesic distances approximated from the 5-NN graph. C+E is directly given these dissimilarities as input whereas t-SNE is only given  $\{x_i\}_{i=1}^n$  as input. To be fair, we also evaluate each embedding against the Euclidean distances in the original space.

Method	Parameters	Spearman	Normalized Stress
C+E (Isomap)	$\alpha = 1$	$0.749 \pm 0.009$	$1.779 \pm 0.075$
C+E (Isomap)	$\alpha = 1.15$	$0.759 \pm 0.010$	$2.022 \pm 0.181$
C+E (LOE)	$\alpha = 2.00$	$0.754 \pm 0.009$	$3.469 \pm 0.103$
t-SNE	$u = 20$	$0.753 \pm 0.029$	$0.714 \pm 0.095$
t-SNE	$u = 550$	<b><math>0.857 \pm 0.006</math></b>	$0.697 \pm 0.007$
Isomap	$q = 5$	0.708	1.199
PCA	-	0.670	<b>0.687</b>

Table 14: Cluster-level metrics on the Human Brain dataset averaged over 5 runs using Euclidean distance to measure pairwise dissimilarity of the original data

Method	Parameters	Spearman	Normalized Stress	Class Preservation
C+E (Isomap)	$\alpha = 1$	$0.829 \pm 0.003$	$3.409 \pm 0.005$	$0.913 \pm 0.019$
C+E (Isomap)	$\alpha = 1.15$	$0.832 \pm 0.009$	$4.020 \pm 0.024$	$0.896 \pm 0.009$
C+E (LOE)	$\alpha = 2.00$	$0.807 \pm 0.009$	$6.519 \pm 0.030$	$0.866 \pm 0.029$
t-SNE	$u = 20$	$0.598 \pm 0.040$	$1.105 \pm 0.036$	$0.758 \pm 0.087$
t-SNE	$u = 550$	$0.852 \pm 0.003$	<b><math>0.396 \pm 0.006</math></b>	$0.910 \pm 0.000$
Isomap	$q = 5$	0.831	2.815	0.943
PCA	-	<b>0.903</b>	0.408	<b>0.959</b>

Table 15: Global metrics on the Human Brain dataset averaged over 5 runs using Euclidean distance to measure pairwise dissimilarity of the original data

**Additional Example: Fashion MNIST** We test our method on 5000 random examples from the Fashion MNIST dataset [40]. For the C+E approach, we use set  $\delta_{ij}$  to the geodesic distances approximated from the 5-NN graph and use the Leiden algorithm to obtain 10 clusters.

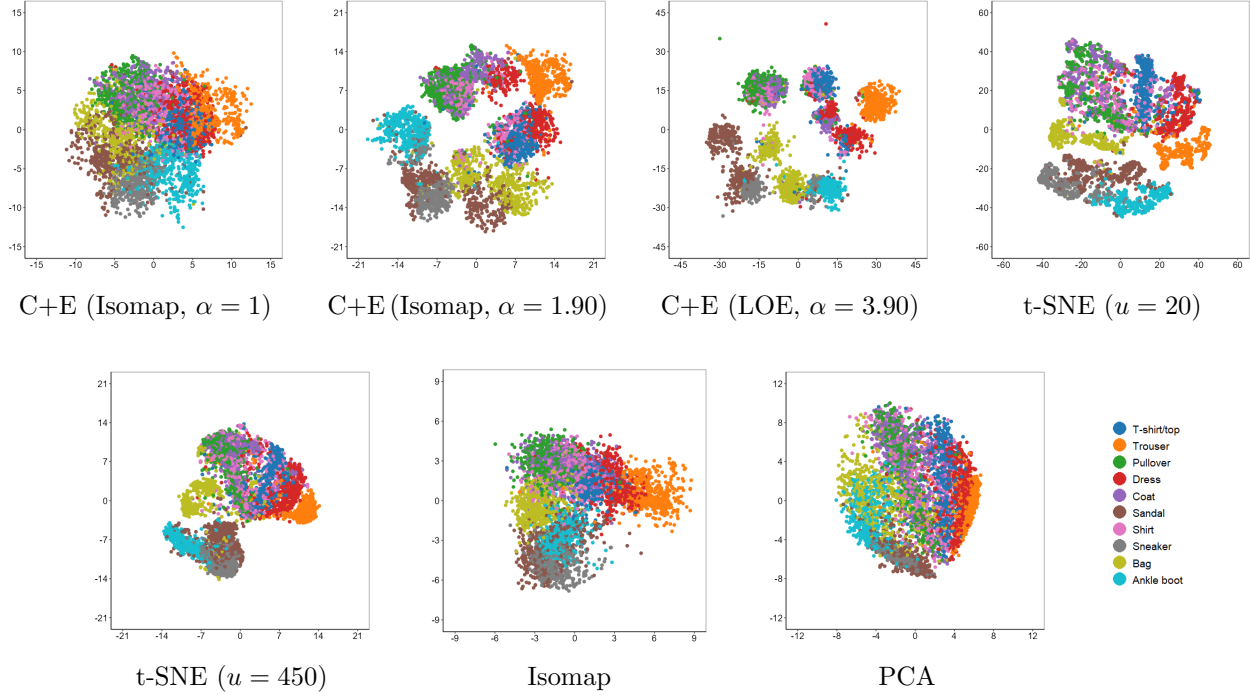


Figure B.3: Embedding of the FMNIST dataset. Points are colored by class label which were not used by the embedding methods.

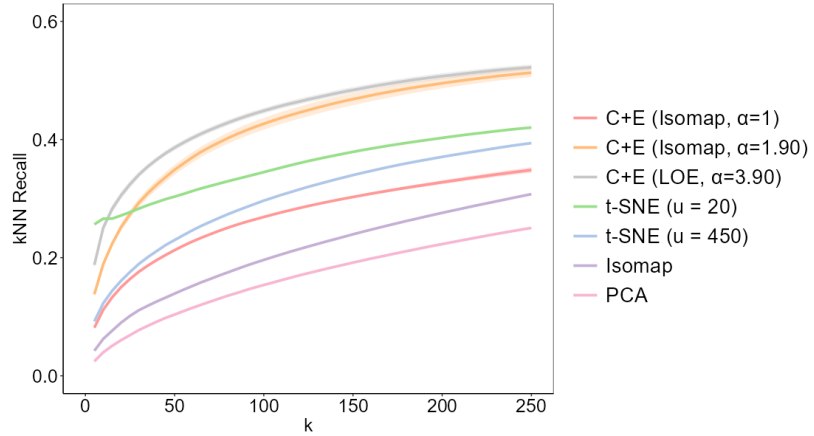


Figure B.4:  $k$ NN recall for the FMNIST dataset for various values of  $k$  for all methods compared averaged over 5 runs.

Method	Parameters	Spearman	Normalized Stress
C+E (Isomap)	$\alpha = 1$	$0.580 \pm 0.023$	<b><math>0.438 \pm 0.011</math></b>
C+E (Isomap)	$\alpha = 1.90$	<b><math>0.617 \pm 0.016</math></b>	$0.602 \pm 0.065$
C+E (LOE)	$\alpha = 3.90$	$0.584 \pm 0.009$	$1.918 \pm 0.394$
t-SNE	$u = 20$	$0.483 \pm 0.009$	$2.311 \pm 0.066$
t-SNE	$u = 450$	$0.418 \pm 0.001$	$0.541 \pm 0.002$
Isomap	$q = 5$	0.439	0.687
PCA	-	0.283	0.572

Table 16: Cluster-level metrics on the FMNIST dataset averaged over 5 runs.

Method	Parameters	Spearman	Normalized Stress	Class Preservation
C+E (Isomap)	$\alpha = 1$	$0.576 \pm 0.005$	<b><math>0.356 \pm 0.002</math></b>	$0.813 \pm 0.017$
C+E (Isomap)	$\alpha = 1.90$	$0.562 \pm 0.035$	$0.906 \pm 0.004$	$0.733 \pm 0.140$
C+E (LOE)	$\alpha = 3.90$	$0.504 \pm 0.058$	$2.690 \pm 0.012$	$0.623 \pm 0.178$
t-SNE	$u = 20$	$0.536 \pm 0.009$	$3.927 \pm 0.037$	$0.691 \pm 0.017$
t-SNE	$u = 450$	$0.566 \pm 0.002$	$0.646 \pm 0.032$	$0.808 \pm 0.006$
Isomap	$q = 5$	<b>0.673</b>	0.485	<b>0.875</b>
PCA	-	0.455	0.393	0.797

Table 17: Global metrics on the FMNIST dataset averaged over 5 runs.

**Additional Example: Single-cell Data II** We use the adult mouse cortex data from [30], with the same preprocessing as in [15]. The original dataset contains 133 clusters labeled by the authors. We restrict our sample of 5000 points to only the inhibitory neurons, which comprise 60 of the clusters. For the C+E approach we set  $\delta_{ij}$  to the geodesic distances approximated from the 10-NN graph and use the Leiden algorithm to cluster the data. We obtain 85 clusters, 64 of which only contain a single data point and we discard these points from the visualization. This leaves 4933 datapoints and 21 clusters with a Rand index of 0.958 with the original labels. For this example only, we fix the clustering across all 5 runs reported in the table.

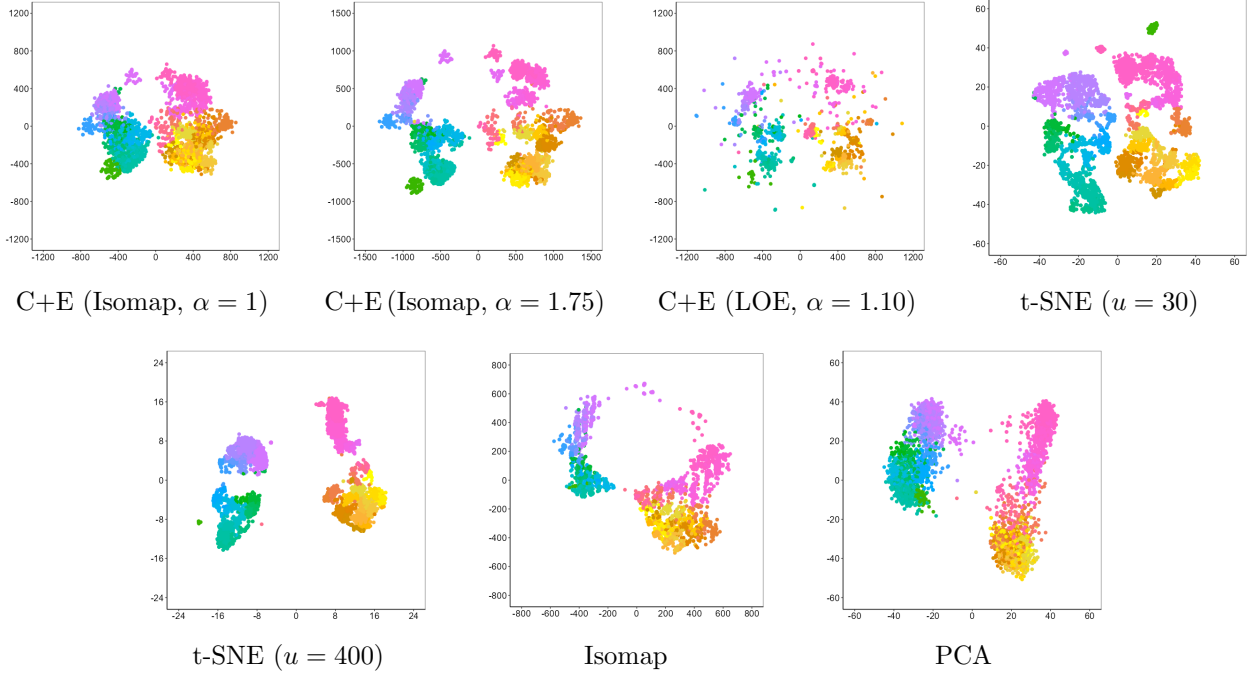


Figure B.5: Embedding of the mouse cortex dataset. Points are colored by class label which were not used by the embedding methods.

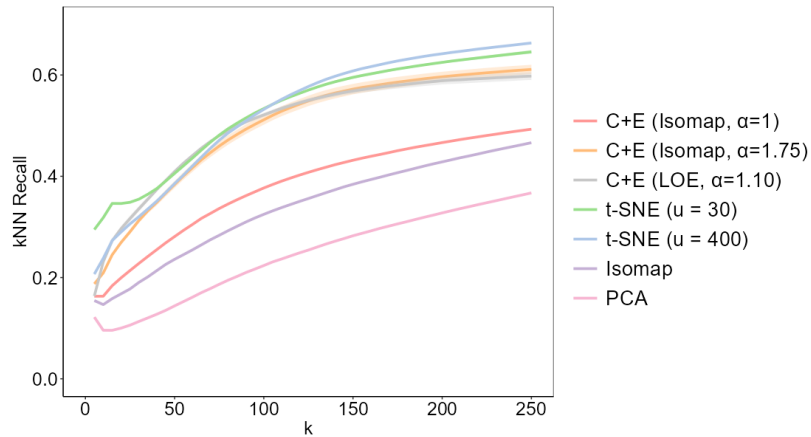


Figure B.6:  $k$ NN recall for the mouse cortex dataset for various values of  $k$  for all methods compared averaged over 5 runs.

Method	Parameters	Spearman	Normalized Stress
C+E (Isomap)	$\alpha = 1$	$0.471 \pm 0.000$	<b><math>0.521 \pm 0.000</math></b>
C+E (Isomap)	$\alpha = 1.75$	$0.476 \pm 0.004$	$0.606 \pm 0.005$
C+E (LOE)	$\alpha = 1.10$	<b><math>0.493 \pm 0.012</math></b>	$0.863 \pm 0.027$
t-SNE	$u = 30$	<b><math>0.493 \pm 0.008</math></b>	$0.975 \pm 0.001$
t-SNE	$u = 400$	$0.449 \pm 0.008$	$0.993 \pm 0.000$
Isomap	$q = 10$	0.322	0.652
PCA	-	0.278	0.960

Table 18: Cluster-level metrics on the mouse cortex dataset averaged over 5 runs.

Method	Parameters	Spearman	Normalized Stress	Class Preservation
C+E (Isomap)	$\alpha = 1$	$0.934 \pm 0.000$	<b><math>0.178 \pm 0.000</math></b>	$0.917 \pm 0.000$
C+E (Isomap)	$\alpha = 1.75$	<b><math>0.938 \pm 0.011</math></b>	$0.757 \pm 0.001$	$0.925 \pm 0.016$
C+E (LOE)	$\alpha = 1.10$	$0.921 \pm 0.001$	$0.223 \pm 0.000$	$0.923 \pm 0.001$
t-SNE	$u = 30$	$0.642 \pm 0.079$	$0.944 \pm 0.002$	$0.659 \pm 0.068$
t-SNE	$u = 400$	$0.781 \pm 0.032$	$0.973 \pm 0.001$	$0.788 \pm 0.026$
Isomap	$q = 10$	0.955	0.213	<b><math>0.943</math></b>
PCA	-	0.761	0.928	0.784

Table 19: Global metrics on the mouse cortex dataset averaged over 5 runs.